Negative Radial Anisotropy Absent Below Cratons: Insights from Bayesian Inversion

S12F-0198

[1]Alistair Boyce, [1]Thomas Bodin, [1]Stephanie Durand, [1]Dorian Soergel

[1]Université Claude Bernard Lyon 1, ENS de Lyon, CNRS, UMR 5276 LGL-TPE, F-69622, Villeurbanne, France

1 Overview

- Global radial anisotropic models are inconsistent (Fig. 1) meaning geological interpretation of active/ancient mantle flow/deformation is challenging.
- One recent interpretation (Priestley et al., 2020) suggests that negative radial anisotropy in the CAM2016 model at ~150km depth within cratons reflects their formation by horizontal shortening/vertical thickening. This mechanism is not easily reconciled with other available models however.
- Using variable parameterizations within both LSQR and Bayesian inversions of Rayleigh and Love (R&L) surface wave dispersion curves, we test whether negative radial anisotropy is reliably recovered at upper mantle depths using synthetic models (Section 3) and whether anisotropic anomalies are required below cratons using real data inversions (Section 4).
- Both algorithmic and parameterization choices can affect 'recovered' radial anisotropy (Xi) meaning existing geological interpretations may be biased.
- Benchmarking against 'active' mid-ocean ridge, hotspot & active mountain belt locations (Fig. 2) available on request.

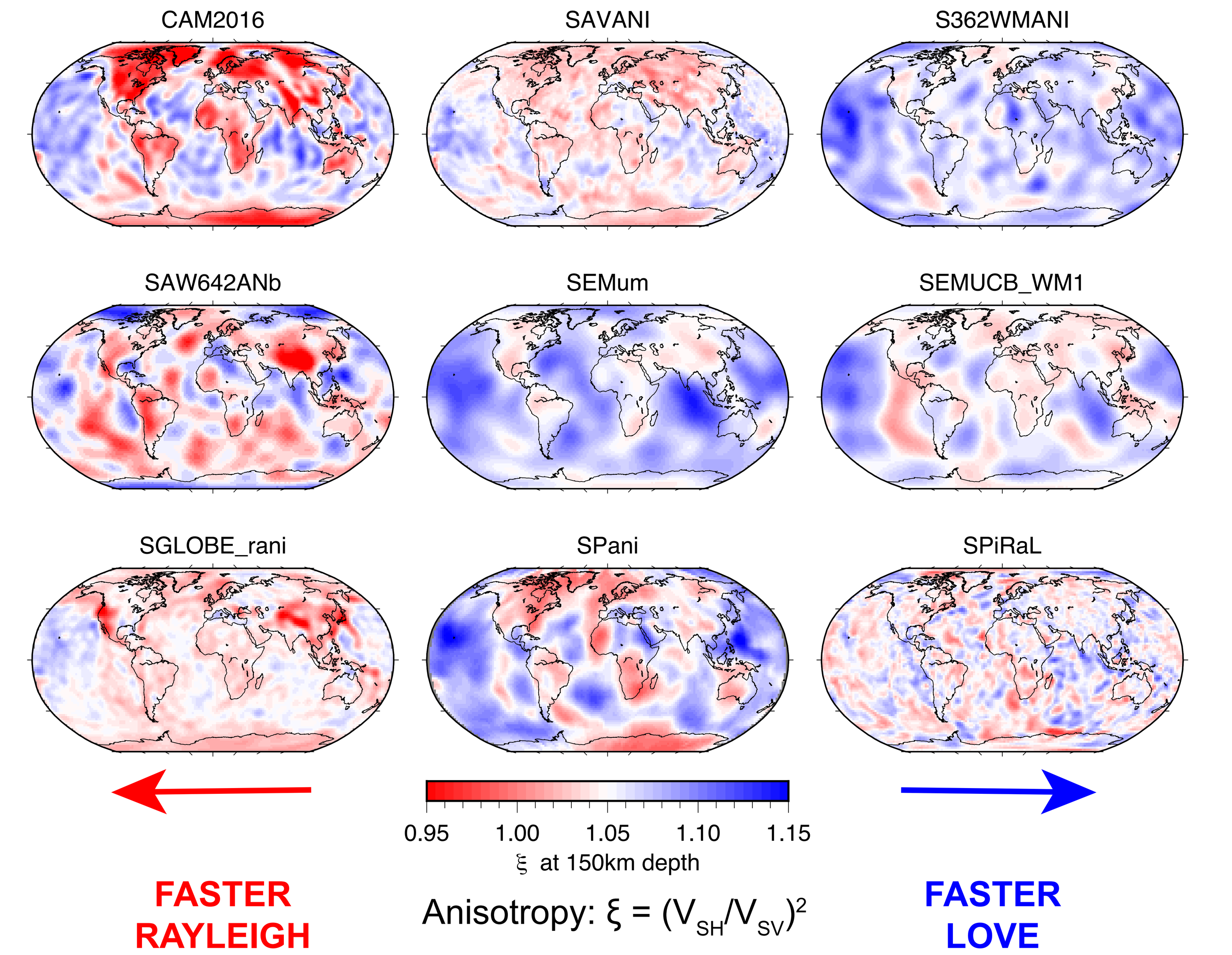

FIGURE 1: Nine published global radial anisotropic models (see references) at 150km depth plotted on a diverging color scale around Xi=1.05, the approximate Xi in PREM at 150km depth.

2 Methodologies

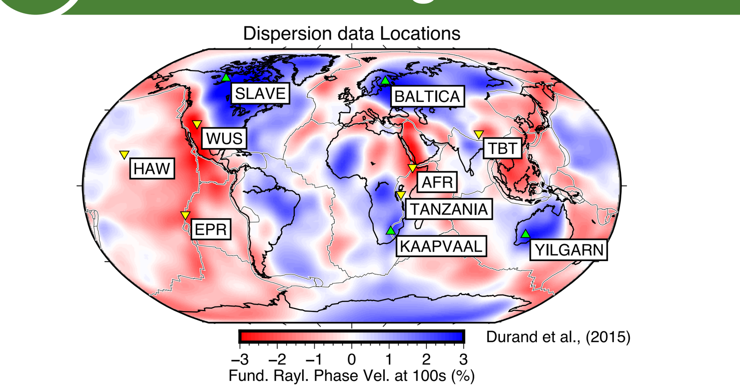

FIGURE 2: Fundamental mode Rayleigh wave phase velocity map at 100s period (Durand et al., 2015) w.r.t. mean value. Locations of cratonic data inversions in Section 4 (green triangles) and 'tectonically active' region data for benchmarking (yellow triangles) are indicated.

- Reference model for all inversions: Modified PREM **without** 220km discont. & upper mantle radial anisotropy, **35km depth Moho**.
- Sensitivity kernels (LSQR) & R&L dispersion curve forward modeling (Bayesian & synthetic models): **Mineos** (Masters et al., 2011).
- **2D LSQR inversion** based on Tarantola & Valette (1982) adapted from Debayle & Ricard (2012). Conservative regularization parameters chosen on L-curve.
- **2D** hierarchical transdimensional **Bayesian inversion** to 700km depth using reversible jump Markov chain Monte Carlo sampling (adapted from Bodin et al., 2016). Number of layers, presence/absence of anisotropy & data error are all free parameters. Prior: +/-20% for V_{SV}, +/-40% for Xi & V_{PH}.

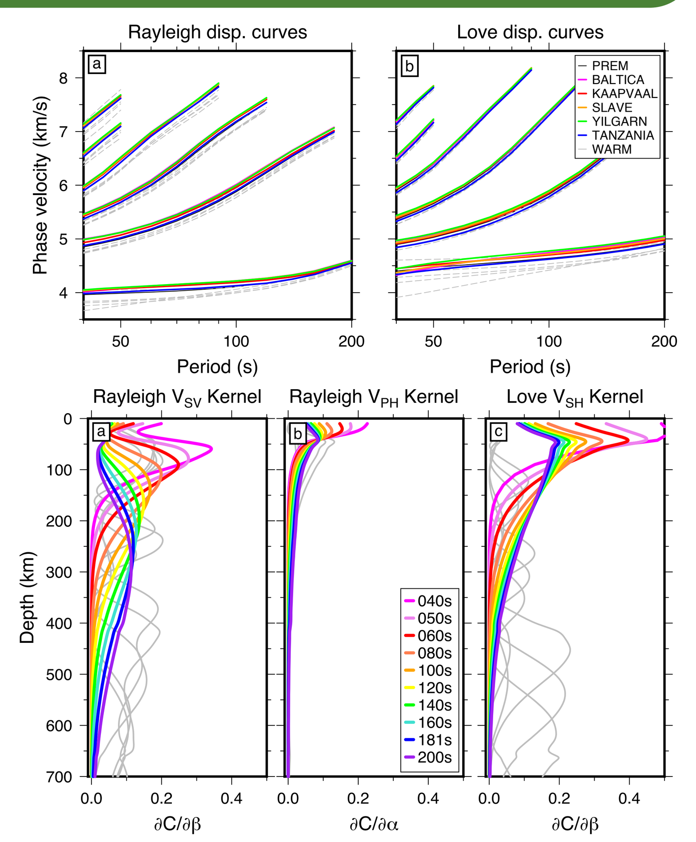

FIGURE 3 (upper): Rayleigh & Love (a,b) fundamental mode and overtone (1-5) dispersion curve data extracted from phase velocity maps (Durand et al., 2015) at 40-200s period at four cratonic locations (colored see Section 4) and 'tectonically active' locations (grey).
FIGURE 4 (lower): Fundamental mode (colored) and 3rd overtone (grey) sensitivity kernels for Rayleigh (V_{SV} & V_{PH}, a,b) and Love (V_{SH}, c) waves at a range of periods for modified PREM reference model.

- **Fundamental & higher mode** (up to 5th overtone) **R&L dispersion curves** at **40-200s period** extracted from phase velocity maps (Durand et al., 2015) at 4 cratonic locations (Figs. 2&3) for inversion in Section 4.

3 Synthetic Data Inversions

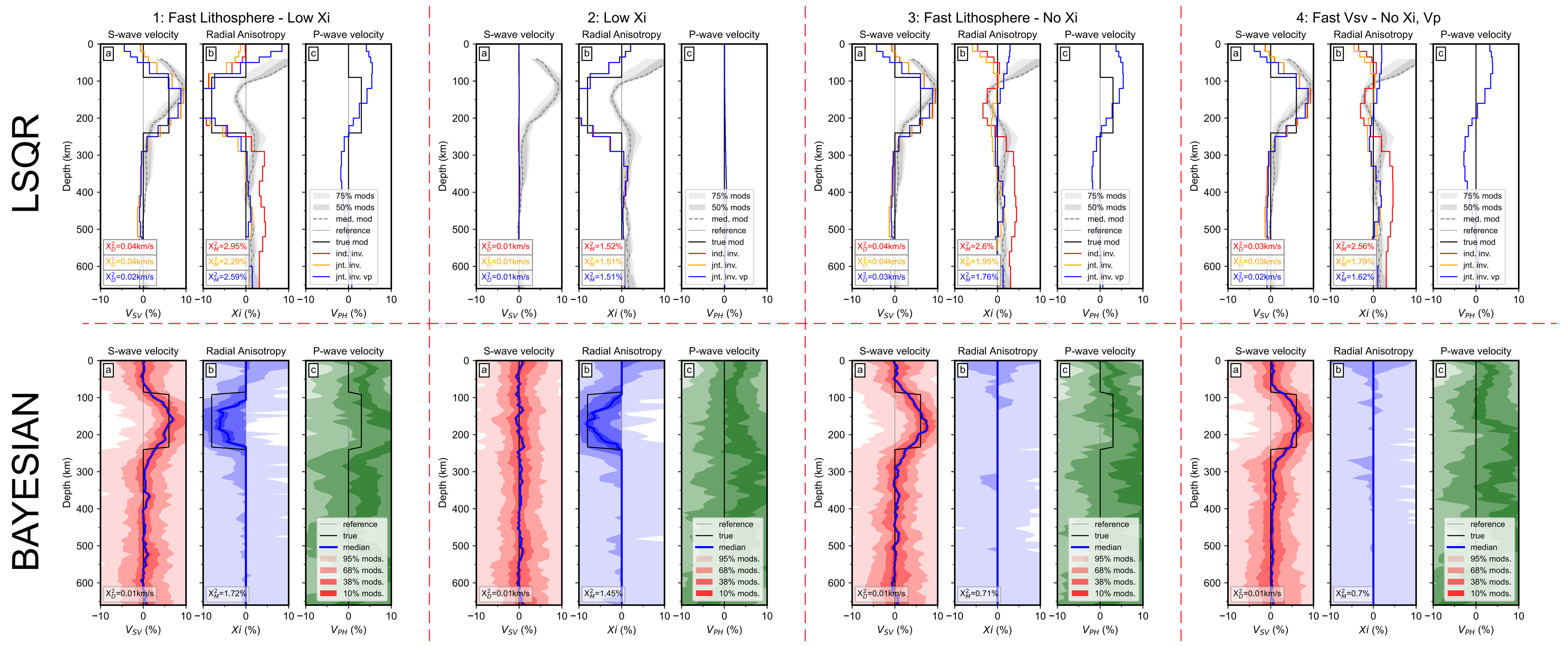

FIGURES 5-8 (Above, Upper): Four synthetic models inverted using variably parameterized LSQR algorithm. V_{SV}, Xi & V_{PH} shown in percent deviation from reference model (no anisotropy). Red curve: Independent inversion for V_{SV} & V_{SH}, Orange curve: Joint inversion for V_{SV} & V_{SH}, Blue curve: Joint inversion for V_{SV}, V_{SH} & V_{PH}. Chi squared data (X^2_D) and model (X^2_M for V_{SV} & Xi) fits shown. Grey line: Reference model, Black line: True model. Grey shaded regions and dashed curve (med. mod) show distribution of V_{SV} & Xi profiles from CAM2016 model (Priestley et al., 2020) extracted at cratonic locations explored in Section 4.

- LSQR: Independent inversions for V_{SV} & V_{SH} produce negative radial anisotropy at ~100-250km depth even for input models with no Xi anomalies. This issue is reduced in joint inversions.
- Data & model fit improves with joint inversions, especially when V_{PH} is a free parameter.
- Bayesian: Substantial improvement in data and model fit for synthetic inversions, assisted by lack of shallow mantle & crustal artefacts.
- V_{SV} & Xi models well recovered. Negative Xi artefacts not seen. True V_{PH} model inside 1 S.D.

FIGURES 9-12 (Above, Lower): Synthetic models inverted using Bayesian algorithm. Posterior distribution (credible intervals) of V_{SV}, Xi & V_{PH} shown in percent deviation from reference model (no anisotropy). Blue curve: Median model. Chi squared data (X^2_D) and model (X^2_M for V_{SV} & Xi) fits shown. Grey line: Reference model, Black line: True model.

4 Real Data Inversions

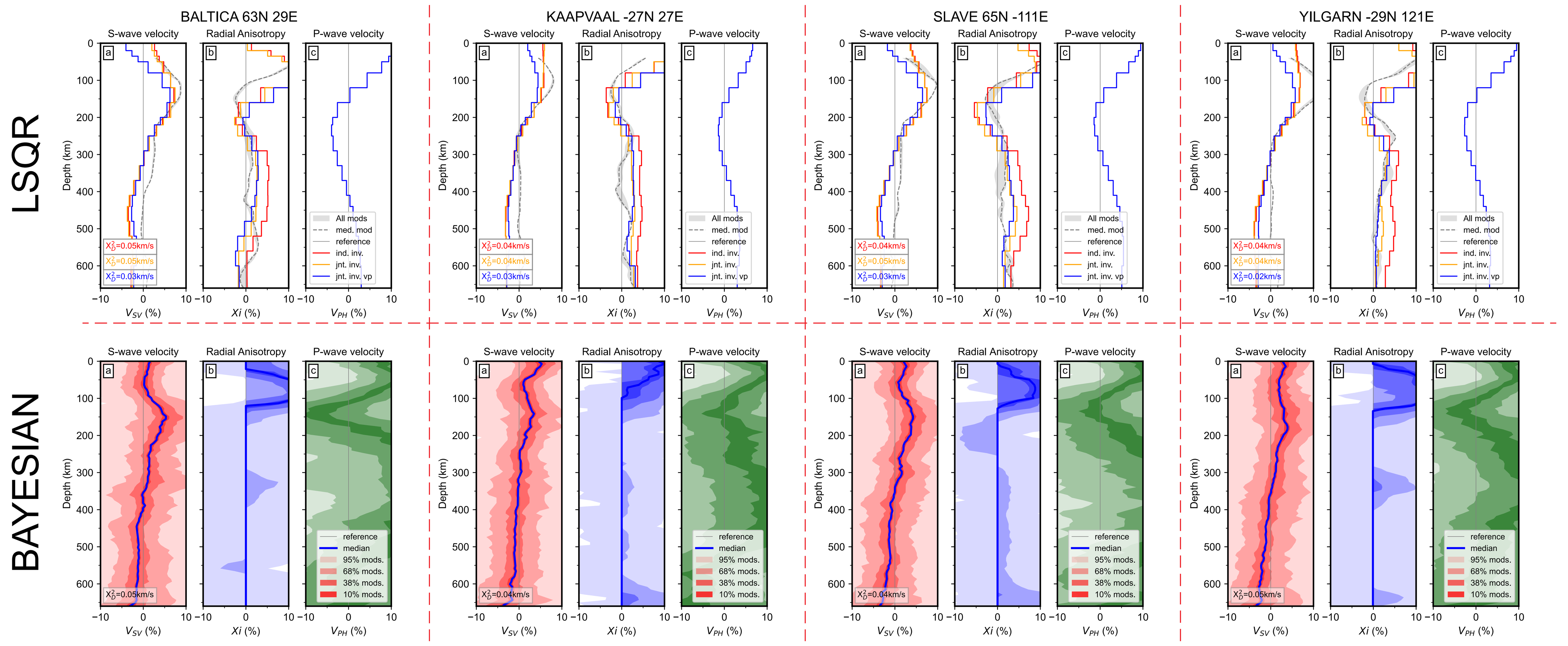

FIGURES 13-16 (Above, Upper): Four cratonic R&L dispersion curves (Fig. 3, Durand et al., 2015) inverted using variably parameterized LSQR algorithm. V_{SV}, Xi & V_{PH} shown in percent deviation from reference model (no anisotropy). Red curve: Independent inversion for V_{SV} & V_{SH}, Orange curve: Joint inversion for V_{SV} & V_{SH}, Blue curve: Joint inversion for V_{SV}, V_{SH} & V_{PH}. Chi squared data (X^2_D) fits shown. Grey line: Reference model, Grey shaded regions and dashed curve (med. mod) V_{SV} & Xi profiles from CAM2016 model (Priestley et al., 2020) extracted at each location.

- LSQR: Variable parameterizations are well fit to CAM2016 V_{SV} & Xi profiles for cratonic locations. Negative Xi at ~150-200km depth is strongest with independent V_{SV} & V_{SH} inversion but is reduced using joint inversions especially with V_{PH} free (while data fit improves).
- Bayesian: Free V_{PH} parameterization shows no negative anisotropy below cratons. +5-10% Xi anomaly is pervasive at <150km depth in the mantle, similarly to PREM.
- V_{SV} reduction or base of positive Xi anomaly associated with mid-lithospheric discontinuity?
- Fast V_{SV} extends >100km deeper than positive Xi anomaly. Highest lithospheric V_{SV} anomaly (~150km depth) occurs at or below base of positive Xi anomaly. Evidence for multiple layers?

FIGURES 17-20 (Above, Lower): Cratonic R&L dispersion curves (Fig. 3, Durand et al., 2015) inverted using Bayesian algorithm. Posterior distribution (credible intervals) of V_{SV}, Xi & V_{PH} shown in percent deviation (+/-10%) from reference model (no anisotropy). Blue curve: Median model. Chi squared data (X^2_D) fits shown. Grey line: Reference model.

5 Methodological Verification

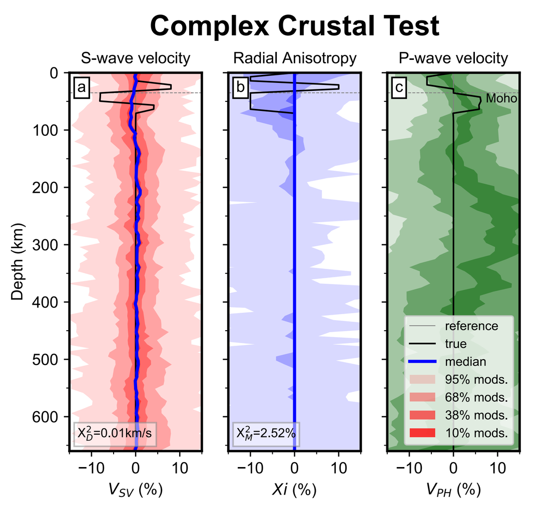

- Synthetic 'Complex Crustal' input model inverted in Bayesian algorithm (Fig. 21).
- Data set (40-200s period) has low sensitivity to crustal structure, and we invert to the surface, meaning artefacts are not mapped into V_{SV} & Xi in the mantle (Fig. 21).
- Further testing shows inaccurate Moho depth (>20km) in reference model produces artefacts in V_{SV} & Xi in the mantle (e.g., Meier et al., 2007, Bozdağ & Trampert, 2008, Chang and Ferreira, 2017).

FIGURE 21 (Above): Synthetic complex crustal model inverted using Bayesian algorithm. Posterior distribution (credible intervals) of V_{SV}, Xi & V_{PH} shown in percent deviation from reference model (no anisotropy). Blue curve: Median model. Chi squared data (X^2_D) and model (X^2_M for V_{SV} & Xi) fits shown. Grey line: Reference model, Black line: True model. Horizontal dashed grey line: 35km depth Moho in true and reference models.

- Posterior sensitivity to scaling of P-wave radial anisotropy, Phi (**Φ**), to S-wave radial anisotropy, Xi (**ξ**), tested by inverting Baltica craton data with variable parameterization **Φ = 1 and Φ =1/ξ** (Figs. 22 & 23).

$$\Phi = (V_{PV} / V_{PH})^2$$

- Minor differences in V_{SV} profile above 300km depth, location of peak anomaly amplitude (~150km depth) is consistent between parameterizations.
- Depth extent of shallow lithospheric positive Xi anomaly consistent but peak amplitude at ~100km depth reduced from Xi>10% (Fig. 22) to Xi>5% (Fig. 23).
- Parameterization choices not likely precluding visibility of negative radial anisotropy.

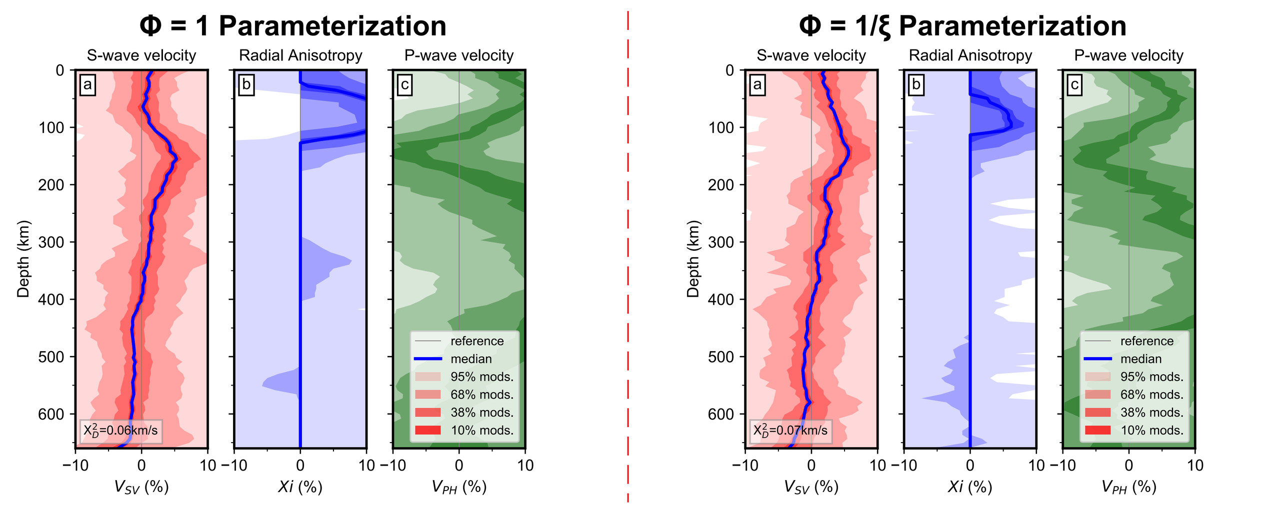

FIGURE 22 (Above, Left): As Fig. 17, Baltica cratonic R&L dispersion curves inverted using Bayesian algorithm. P-wave radial anisotropy parameter fixed: Phi = 1. Posterior contains 25% of the number of samples in Fig. 17. Posterior distribution (credible intervals) of V_{SV}, Xi & V_{PH} shown in percent deviation (+/-10%) from reference model (no anisotropy). Blue curve: Median model. Chi squared data (X^2_D) fits shown. Grey line: Reference model.

FIGURE 23 (Above, Right): Same as Fig. 22 but with scaled P-wave radial anisotropy parameter: Phi = 1/Xi.

TAKE-HOME MESSAGES

1. **Negative Xi below cratons** (~150km depth), reproduced using LSQR inversion, is **likely an artefact**…
2. **Bayesian inversion** with free V_{PH} parameterization yields **no negative radial anisotropy below cratons**, only +5-10% Xi above 150km depth, similar to PREM.
3. **Episodic craton formation** (e.g., Yuan & Romanowicz 2010; Darbyshire et al., 2013) **preferred** over horizontal shortening (Priestley et al., 2020).
4. **Set V_{PH} free** in surface wave inversions, preferably with Bayesian algorithms!

Funding statement:
This work received funding from the **European Research Council** (ERC) under the European Union's Horizon 2020 research and innovation programme (grant agreement No. 716542-TRANSCALE) and is supported by the **Centre National de la Recherche Scientifique** at unit UMR5276 (LGL-TPE).

References:
Bodin, T., et al., (**2016**) *Geophys. J. Int.* doi: 10.1093/gji/ggw124. Bozdağ, E. & Trampert, J. (**2008**) *Geophys. J. Int.* doi: 10.1111/j.1365-246X.2007.03690.x. Chang, S. & Ferreira, A.M.G. (**2017**) *B. Seismol. Soc. Am.* doi: 10.1785/0120160142. Darbyshire, F.A. et al., (**2013**) *Earth Planet. Sci. Lett.* doi: 10.1016/j.epsl.2013.05.002. Debayle, E. & Ricard, Y. (**2012**) *J. Geophys. Res.* doi: 10.1029/2012jb009288. Durand, S., et al., (**2015**) *Geophys. Res. Lett.* doi: 10.1002/2015gl063700. Masters, G. et al., (**2011**), *Mineos v1.0.2, Computational Infrastructure for Geodynamics*, url: https://geodynamics.org/cig. Meier, U. et al., (**2007**) *Geophys. Res. Lett.* doi: 10.1029/2007gl030989. Tarantola, A. & Valette, B. (**1982**) *Rev. Geophys.* doi: 10.1029/RG020i002p00219. Yuan, H. and Romanowicz, B. (**2010**) *Nature* doi: 10.1038/nature09332. ***Xi Models:*** ***CAM2016***: Priestley, K. et al., (**2020**) *Geology*, doi: 10.1130/G47696.1. ***SAVANI***: Porritt, R.W., et al., (**2021**) *Geophys. J. Int.* doi: 10.1093/gji/ggab185. ***S362WMANI***: Kustowski, B,G. et al., (**2008**), *J. Geophys. Res.*, doi: 10.1029/2007JB005169. ***SAW642ANb***: Panning, M.P., et al., (**2010**). *J. Geophys. Res.* doi: 10.1029/2010JB007520. ***SEMum***: Lekic, V. & Romanowicz, B. (**2011**) *Geophys. J. Int.* doi: 10.1111/j.1365-246X.2011.04969.x. ***SEMUCB_WM1***: French, S.W. & Romanowicz, B. (***2014***) *Geophys. J. Int.* doi: 10.1093/gji/ggu334. ***SGLOBE-rani***: Chang, S.-J. et al., (**2015**) *J. Geophys. Res.*, doi: 10.1002/2014JB011824. ***SPani***: Tesoniero, A., et al., (**2015**), *J. Geophys. Res.* doi: 10.1002/2015JB012026. ***SPiRaL***: Simmons N.A., et al., (**2021**) *Geophys. J. Int.* doi: 10.1093/gji/ggab277.

alistair.boyce@univ-lyon1.fr / @alistair_boyce / alistairboyce11.github.io